Energy Conversion and Management 263 (2022) 115705

Contents lists available at ScienceDirect

Energy Conversion and Management

journal homepage: www.elsevier.com/locate/enconman

Energy savings potential of reversible photothermal windows with near infrared-selective plasmonic nanofilms

Md Anwar Jahid [a], Julian Wang [a,*], Enhe Zhang [a], Qiuhua Duan [b], Yanxiao Feng [a]

[a] Department of Architectural Engineering, Penn State University, United States
[b] Department of Civil, Construction and Environmental Engineering, University of Alabama, United States

ARTICLE INFO

Keywords:
Dynamic window
Reversible window
Solar infrared
Solar heat gain
Building energy
Photothermal
Nanofilm
Surface plasmon resonance

ABSTRACT

A variety of dynamic window and glazing systems with variable solar heat gain control features reacting to seasonal weather conditions and indoor space heating and cooling demands have been investigated in the past several decades. However, the modulation of solar heat gain has to affect the solar light transmittance in most existing dynamic glazing and window systems. In this work, a new type of dynamic window concept was proposed: reversible photothermal windows based on nanoscale solar infrared-induced plasmonic photothermal effects, which can modulate solar heat, independent of visible light conditions. This study provides the underlying technical characteristics and the thermal and optical features under solar irradiation via experimentally validated analytical models. The reversible photothermal windows exhibit a substantial ability to control solar heat gain coefficient with a range between about 0.2 and 0.6 and a stable visible transmittance of 0.32, A whole-building energy simulation demonstrates the potential for energy savings offered by reversible photothermal windows could reach over 18% in mixed climates, as compared to baseline models built using the most recent energy efficiency standards. This research illustrates technical and numerical evidence and mechanisms for energy savings that will support future research and development of this new dynamic window technology.

1. Introduction

The energy efficiency of building windows is a very important factor to consider. Heat loss and gain through traditional windows are responsible for around 40% of building energy consumption [1]. According to the Lawrence Berkeley National Laboratory (LBNL), upgrading current windows to energy-saving windows could save more than 1 quadrillion Btu [2]. Energy-efficient windows greatly influence the resulting building performance, such as through thermal management, the regulation of daylight [3], solar and ambient air energy capture, and glare reduction [4]. In this context, two performance metrics primarily contribute to overall building energy use: the overall heat transfer coefficient (U-factor) and solar heat gain coefficient (SHGC), which are associated with thermal conduction and solar gain through windows, respectively. Particularly during the heating and cooling seasons, for residential and commercial buildings alike, solar heat gain through windows represents about 3.1 quads of primary energy use. This is similar to the thermal conduction effects on energy use and represents almost 20% of envelope-related energy use [5]. Importantly, solar heat gain is clearly seasonal. Solar heat gain through building windows can offset heating energy use in the winter and blocking unwanted solar heat through windows can result in improved comfort and reduced cooling energy use [6]. Modulation of sunlight (often called solar radiation) has become a significant factor in contemporary energy-efficient windows [7]. Representative glazing technologies for such purposes include low-e coatings [8], micro-blinds [9], dielectric/metal films [10], photothermal coatings [11], electrochromic glazing [12], gasochromic window [13], liquid crystal glazing's [14], and thermochromic window [15], and phase change materials (PCM)-integrated glazings [16].

In particular, transmitted solar heat gain can be controlled by designing and adjusting the solar reflective and/or absorptive properties of windows.

- **Solar Reflection:** From the solar reflection perspective on solar heat gain modulation, the most representative technology is low-e coatings. Low-e coatings are spectrally selective layer structures that let most visible light pass through but reflect the near-infrared (NIR)

Abbreviations: U-factor, Overall Heat Transfer Coefficient; SHGC, Solar Heat Gain Coefficient; PPE, Plasmonic Photothermal Effect; NIR, Near-Infrared; LSPR, Local Surface Plasmon Resonance; SHGC, Solar heat gain coefficient.

* Corresponding author.
E-mail address: julian.wang@psu.edu (J. Wang).

https://doi.org/10.1016/j.enconman.2022.115705

Available online 12 May 2022

Nomenclature

Q_{in}	Absorbed solar irradiance
Q_{out}	Dissipative heat transfer
$Q_{solar\ gains}$	Absorbed solar-driven inward-flowing heat transfer
$Q_{u\text{-}factor}$	U-factor-driven heat transfer
$T_{glass,s}$	Glass surface temperature
T_{NPs}	Coated layer's surface temperature
T_{∞}	Ambient air temperature
T_o	Outdoor temperature
R_h	Interfacial insulation
h_{con}	Conductive heat transfer coefficient
T_i	Indoor temperature
$T_{in,s}$	Inner surface temperature of windows
G_λ	Incident spectral solar irradiance
G_o	Incident solar irradiance

portion of solar energy, the portion primarily responsible for indoor heat generation [17]. This means more daylight and less heat gain. In the last two decades, an enormous amount of research has been done on low-e coatings, due to their high IR reflection properties (around 92%) [18]. There are two types of low-e coatings: silver-based soft coatings and tin oxide-based hard coatings [19]. The former offers higher infrared (IR) reflectance (92%) and lower transmittance than the latter [20], but the visible light transmittance of oxide-based hard coatings can be increased via the anti-reflecting property of silicon dioxide [21]. A quality low-e coated window reduces heat gain from solar radiation, saving up to 47% and 35% of high cooling demand and total energy, respectively [16]. Moreover, low-e coatings' effect on longwave IR enables heat from warmed interiors in winter to be trapped inside, significantly reducing heat loss [22], and maintaining sensible and latent cooling [23].

- **Solar Absorption:** Instead of reflecting solar heat back to the outdoors, the absorption of solar radiation through glazings and window systems can also achieve solar heat gain modulation. The most typical strategy is to use tinted glazings. The addition of metal oxides (e.g., iron, manganese, chromium) to molten glass can form a glass tint, the color of which depends on the metal oxide used. Tinted glazings can boost the solar absorption of glass by 10% (for clear glass) to 60% [24]. Such solar-absorptive windows can significantly reduce the solar radiation transmitted, so solar absorptive smart windows are primarily used for cooling purposes in hot climates and reducing discomfort from glare. For instance, around 47% of cooling energy can be saved in hot climates [17]. However, it is worth mentioning that all absorbed solar radiation is transformed into heat within the structure, thus raising the glass temperature. The surface temperature of tinted glazing is 6.6 °C higher in summer than clear glazing, and the converted thermal energy is eventually transferred to the ambient environment, including the interior [24]. For example, compared to single-pane windows, tinted coatings on the internal layer or windowpane in multi-pane window structures can relatively enhance the inward heat flow [25]. However, analyses have shown that they still reduce solar heat gain because of the significant reduction in transmitted solar heat. This inward-flowing heat is considered in the standardized SHGC calculations, but may not have significant effects on the resultant SHGC values. This feature has been verified in several prior studies [26]. In other words, although the high solar absorption of windows may bring some heat addition to the interior, the reduction of transmitted solar heat gain is much more significant, substantially reducing the solar heat gain overall.
- **Dynamic fashion:** In addition to the above passive solar heat gain control techniques, the last several decades have seen the development of numerous dynamic glazing technologies. The major function of such dynamic controls is switching the solar transmission between high and low levels. This is accomplished during specific seasons by adjusting the solar reflection, absorption, or both (i.e., high reflection and moderately strong solar absorption). For instance, thermochromic materials have been used for smart window applications, due to their spectral variations in response to temperature, switching between clear (i.e., low solar absorption) and tinted states (i.e., high solar absorption). The solar transmittance modulation range can be from around 0.16 (in the dark state) to 0.74 (in the clear state), with visible light transmittance ranging from 16% to 90%, respectively [27]. Compared with plain double-pane glazing, general thermochromic (coated) windows can save 22% energy [27]. Moreover, electrochromic materials have attracted substantial attention for smart window applications, due to their modulation ability in response to a broad spectral range of solar radiation. Similar to thermochromic windows and solar absorption modulation, electrochromic glazings switch among bleached, intermediate, and fully-colored conditions to form dynamic solar transmission that is activated by varying the voltage input. The typical SHGC ranges from 0.10 to 0.50, and the visible transmittance ranges from 0.1 to 0.72, potentially saving building heating and cooling energy by 13.2–21.5% in different climates, as compared to typical static windows [28]. Photochromic materials can change color to the desired wavelength and adjust their solar absorption. The materials offer high photochromic contrast, are reversible and fast-switching, and feature an acceptable range of photochemical stability. The variation ranges of SHGC and visible transmittance of photochromic windows are about 0.11–0.26 and 25–65%, respectively, while they can be designed in different bands [29]. In recent years, some studies have focused on gasochromic windows that produce effects similar to those of electrochromic windows, but are simpler and less expensive because only a single electrochromic layer is sufficient. Their SHGC could range from 0.16 to 0.55, and visible transmittance could range from 29% to 65% [30]. Switchable adaptive polymer dispersed liquid crystal (PDLC) glazing has been developed, and its SHGC range is about 0.63 and 0.68 with a visible transmittance range of 44–79% [31]. Additionally, the SHGC and visible variations in suspended particle device (SPD) glazings could be about 0.11–0.39 and 2–38%, respectively, based on a recent SPD-based vacuum glazing design [32].

However, current state-of-the-art dynamic glazing technologies have to attenuate or enhance both visible and NIR wavelengths to attain dynamic SHGC control. In other words, the visible transmittance has to be significantly reduced when the SHGC drops. Decoupling the solar visible and NIR radiation to enable independent control of daylight and solar heat in winter and summer has been deemed as one of the critical characteristics for future dynamic glazing [5]. Here, a new concept: reversible photothermal windows coated with plasmonic nanofilms that can be flipped for the summer and winter seasons is proposed. As shown in the schematic in Fig. 1, in summer, a windowpane doped with plasmonic nanoparticles (NPs) decreases the solar IR transmitted to the interior by absorbing NIR. The surface-plasmon-mediated photothermal effect mostly occurs in the outer layer, and the absorbed solar heat is primarily released to the exterior. In winter, the window system is reversed to switch the solar NIR-absorbing windowpane such that it faces the interior. The NIR-absorbing windowpane absorbs the transmitted NIR and increases its temperature. Combined with the unique localized heating and insulation ability of the central air layer, the most absorbed thermal energy is retained in the inward direction. In other words, due to the seasonal placement of the plasmonic nanofilms on windows, forming a significantly different inward-flowing fraction of absorbed solar heat is hypothesized, which could substantially affect the overall solar heat gain, independent of visible transmittance.

The 360-degree reversibility of window glazing elements is available

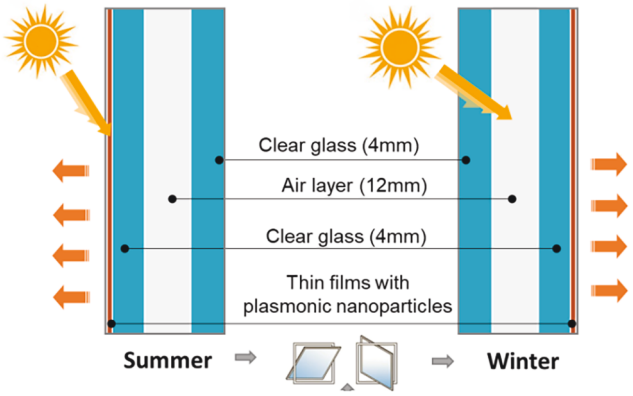

Fig. 1. Schematic of reversible photothermal windows.

on the market, though their purpose at this time is primarily to facilitate easy cleaning rather than energy savings. This study is the first to demonstrate a reversible window concept for dynamic solar heat gain control that is capable of responding to different seasons and offering the related potential for energy savings for heating, cooling, and lighting. This new type of dynamic window relies on the solar NIR-driven plasmonic photothermal effect (PPE) of NPs and its localized surface heating phenomenon. Compared with the existing dynamic window and glazing systems, this proposed technology can uncouple the visible and NIR solar radiation, which enables unprecedented dynamic properties - high SHGC modulation but a stable visible transmittance. Another important contribution of this work is its delineation of the underlying mechanism of this new concept: why and how solar heat gain can be modulated by the unique combination of PPE and the air gap insulation ability of double-pane windows, independent of the visible portion of solar light. This was accomplished through experimentally validated models and numerical analysis. These are presented herein, along with a comprehensive discussion of the applicability of reversible photothermal windows and their potential for energy savings across different climates. This new type of dynamic window, however, could be used to address current challenges in this area, due to its straightforward technicality, high controllability, and the minimal effort needed for building integration, operation, and maintenance.

2. Materials and methods

In this section, the basic principles and theory of using plasmonic nanostructures for designing spectral selectivity in glazing systems are first briefly introduced. Subsequently, the materials and experiments used to develop and validate numerical models are illustrated, in which the governing equations related to the heat transfer with the nanoscale PPE are also presented.

2.1. Plasmonic nanostructures for spectral selectivity in glazings

Spectral selectivity is highly desirable because it can maintain high and stable visible transmittance and mostly handles the solar NIR to which human eyes are not sensitive but typically occupy more than 50% of solar radiation [33]. In recent years, plasmonic nanoparticles (NPs) and nanostructures have attracted substantial attention for use in spectrally-selective glazing systems, due to their optical, chemical, electronic, and catalytic properties. There are three main features of plasmonic nanostructures: electric field enhancement, hot electron generation, and photothermal effects [34]. First, plasmonic NPs or nanostructures are very attractive due to their nanofocusing and local surface plasmon resonance (LSPR) [35]. Within the nanostructures, there is a strong interaction between the collective oscillations of the electron (originating from the light) and metallic nanostructures. The LSPR features of (metallic) plasmonic nanostructures can be adjusted for efficient conversion of electric field enhancement and incident light, and strong confinement around the metallic NPs or nanostructures [36]. Second, plasmonic nanostructures absorb incident photons, producing plasmon-induced hot electrons [37], which can be used to improve the efficiency of optoelectronic devices, due to the excellent intersection between light and metallic nanostructures [38]. When light propagates through plasmonic nanostructures at designated wavelengths [39], free electrons move around on the surfaces of plasmonic antennae [34]. The generation of hot electrons in plasmonic nanostructures extends the detection capability of semiconductors on their band gaps, though semiconductors do not absorb light at desired wavelengths [40]. Third, in the LSPR condition, the free electrons on the NP's surface are highly excited and energetic, but they eventually fall back to the ground state and release extra energy. This relaxation process eventually induces thermal dissipation and exhibits localized heat to the surrounding medium, which is considered to be the plasmonic photothermal effect [41].

Plasmonic nanostructures have been recently applied to window and glazing systems, and their investigation is mainly in two areas: electrochromic plasmonic windows and plasmonic photothermal windows. As compared to other electrochromic materials that normally control visible light [42], recent studies have suggested that plasmonic coatings can offer a unique opportunity to control the transmission of NIR without affecting visible light [43] and also exhibit rapid switching behavior [44]. By using the synergistic interaction between tungsten oxide (WO_{3-x}) nanocrystals and niobium oxid (NbO_x) glass, the electrochromic plasmonic glazing can achieve an independent switch between transmitting and blocking in the NIR at the high SHGC region [45]. However, in the low SHGC region, the system's switching begins to occur strongly in both the visible and NIR regions [46]. Another type of application is related to utilizing the plasmonic photothermal effect (PPE) of nanostructures, exploring the surface plasmon-enhanced or induced characteristics of plasmonic NPs that enable significant and tunable light absorption [47]. The previous research on this topic demonstrated that plasmonic nanofilms on single-pane windows exhibit unique thermal transport features, which may enable the semi-directional thermal management of absorbed solar radiation (Fig. 2). Due to the above-mentioned quasi-ballistic thermal transport feature of plasmonic nanofilms, the inward-flowing heat fraction of the single-pane windows tested was significantly improved relative to conventional or low-e coated single-pane windows. Compared to the various low-e technologies, the energy savings of photothermal windows were determined to be 7.6% to 13.2% of the complete building's heating energy scale. The heat loss prevention was approximately 12.2% to 20.1% and the gain in solar heat was around 14.2% to 16.7%. This was very close to the thermal performance (in the winter season) of double-pane windows receiving traditional solar radiation. However, such PPEs become undesirable during the summer season [47].

2.2. Characterization of materials and coated glazing

The metallic NPs (Fe_3O_4@$Cu_{2-x}S$) were synthesized as in previously published work [48], yielding spectrally-selective absorption of NIR with little reduction in the visible region. To synthesize the Fe_3O_4@$Cu_{2-x}S$ NPs, 60 mL of oleylamine was placed in a three-necked flask and then heated and stirred at 300 °C for 30 min in a gaseous medium (nitrogen). Next, 8 mL of N-methyl-2-pyrrolidone, 12 mL of oleylamine, and 700 mg of Fe $(acac)_3$ were added to the round flask, kept for 10 min at 300 °C, then cooled to 70 °C for another 10 min. Following, 128.28 mg of sulphur was dissolved in 12 mL of oleylamine mixed with 10 mL of cyclohexane and added to the solution in the previously-mentioned flask. After stirring for 10 min at 70 °C, 523.52 mg of Cu $(acac)_2$ was dissolved in 4 mL of oleylamine, and 16 mL of chloroform solution was injected into the solution. The final mixture was stirred for 30 min at 70 °C. Then, the Fe_3O_4@$Cu_{2-x}S$ NPs were collected by a magnet, washed three times with methanol, and freeze-dried. After drying, the NPs were

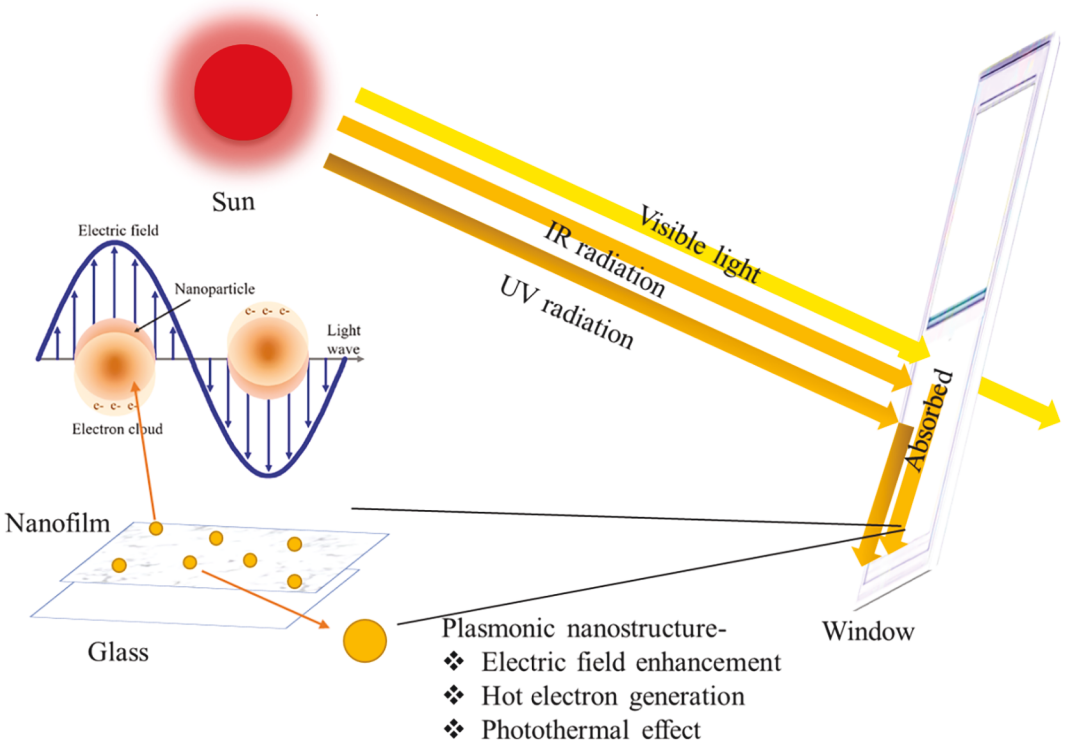

Fig. 2. Modulation of solar radiation by windows incorporating plasmonic nanostructures.

diluted in toluene for future use. The thin-film samples were prepared using 2.54 × 2.54 cm^2 micro-slides, stirred (i.e., sonicated) in acetone for 15 min, stirred in isopropyl alcohol for another 15 min, and dried for 30 min at 50 °C in an isotemp oven (Fisher Scientific 500 series). Toluene solutions containing various $Fe_3O_4@Cu_{2-x}S$ NPs were fixed with 5% PMMA. The solutions were spin-coated onto glass substrates for 10 s at 1,000 rpm. Each glass slide was coated with 80 μL of solution.

Grazing incidence X-ray diffraction (GIXRD) patterns were collected from 6 to 60° 2θ using a Malvern Panalytical Empyrean® instrument fitted with a copper long-fine-focus X-ray tube operated at 45 kV and 40 mA. The incident beam path included a parallel beam X-ray mirror and a 0.5° divergence slit fixed at an incident angle of 1°. The diffracted beam path incorporated dCore® optics with a 0.28° parallel plate collimator and a PIXcel3D® detector operating in open detector (0D) mode with an active length of 14.025 mm. Data were collected with a nominal step size of 0.026° 2θ. There were a series of peaks at two-theta = 16°, 24°, 33.5°, 35°, 40°, and 43° in the patterns of $Fe_3O_4@Cu_{2-x}S$ (Fig. 3). All the diffraction peaks in the XRD pattern could easily be identified as the phase of the $Fe_3O_4@Cu_{2-x}S$ nanoparticle. The peaks at 33.1° degree and 46.6° can be identified as the CuS and peaks at 18.1°, 21.2°, 24.5°, 35.5°, 42.2° can be identified as Fe_3O_4, which also proves the semicrystalline structure of $Fe_3O_4@Cu_{2-x}S$ nanoparticles. To further confirm the presence of different elements in the $Fe_3O_4@Cu_{2-x}S$ nanoparticles, XPS was performed.

X-ray photoelectron spectroscopy (XPS) experiments were performed using a Physical Electronics VersaProbe III instrument equipped with a monochromatic Al kα x-ray source (hν = 1486.6 eV) and a concentric hemispherical analyzer. Charge neutralization was performed using both low-energy electrons (<5 eV) and argon ions. The binding energy axis was calibrated using sputter cleaned Cu ($Cu\ 2p_{3/2}$ = 932.62 eV, $Cu\ 3p_{3/2}$ = 75.1 eV) and Au foils ($Au\ 4f_{7/2}$ = 83.96 eV). Peaks were charged referenced to the CH_x band in the carbon 1 s spectra at 284.8 eV. Measurements were made at a takeoff angle of 45° with respect to the sample surface plane. This resulted in a typical sampling depth of 3–6 nm (95% of the signal originated from this depth or shallower). Quantification was done using instrumental relative sensitivity

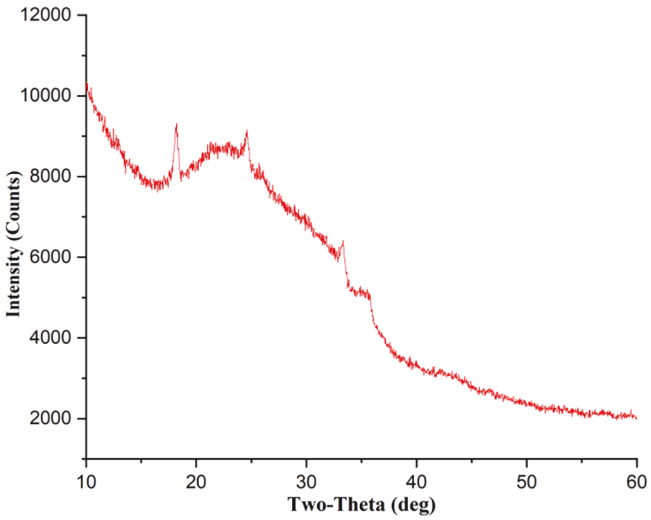

Fig. 3. X-ray diffraction (XRD) of $Fe_3O_4@Cu_{2-x}S$ nanoparticles.

factors (RSFs) that account for the x-ray cross-section and inelastic mean free path of the electrons. On homogeneous samples, major elements (>5 atom%) tend to have standard deviations of < 3% while minor elements can be significantly higher. The analysis size was ~ 200 μm in diameter. To determine the electronic structure and chemical composition of $Fe_3O_4@Cu_{2-x}S$, X-ray photoelectron spectroscopy (XPS) was performed, and the fullspectrum result was shown in Fig. 4. The XPS spectrum of $Fe_3O_4@Cu_{2-x}S$ nanoparticles indicates the presence of $Fe^{2+,3+}$, Cu^{+}, Cu^{2+}, sulfides, disulfides, sulfates, hydrocarbons, C-N, $C-N^{+}$, and COO, which indicates the presence of the different elements of $Fe_3O_4@Cu_{2-x}S$ nanoparticles.

Transmission electron microscopy was used to determine the nanoparticle size. Transmission and absorption spectra were obtained by a UV–VIS-NIR spectrometer Lambda 900 (PerkinElmer Inc.). Table 1

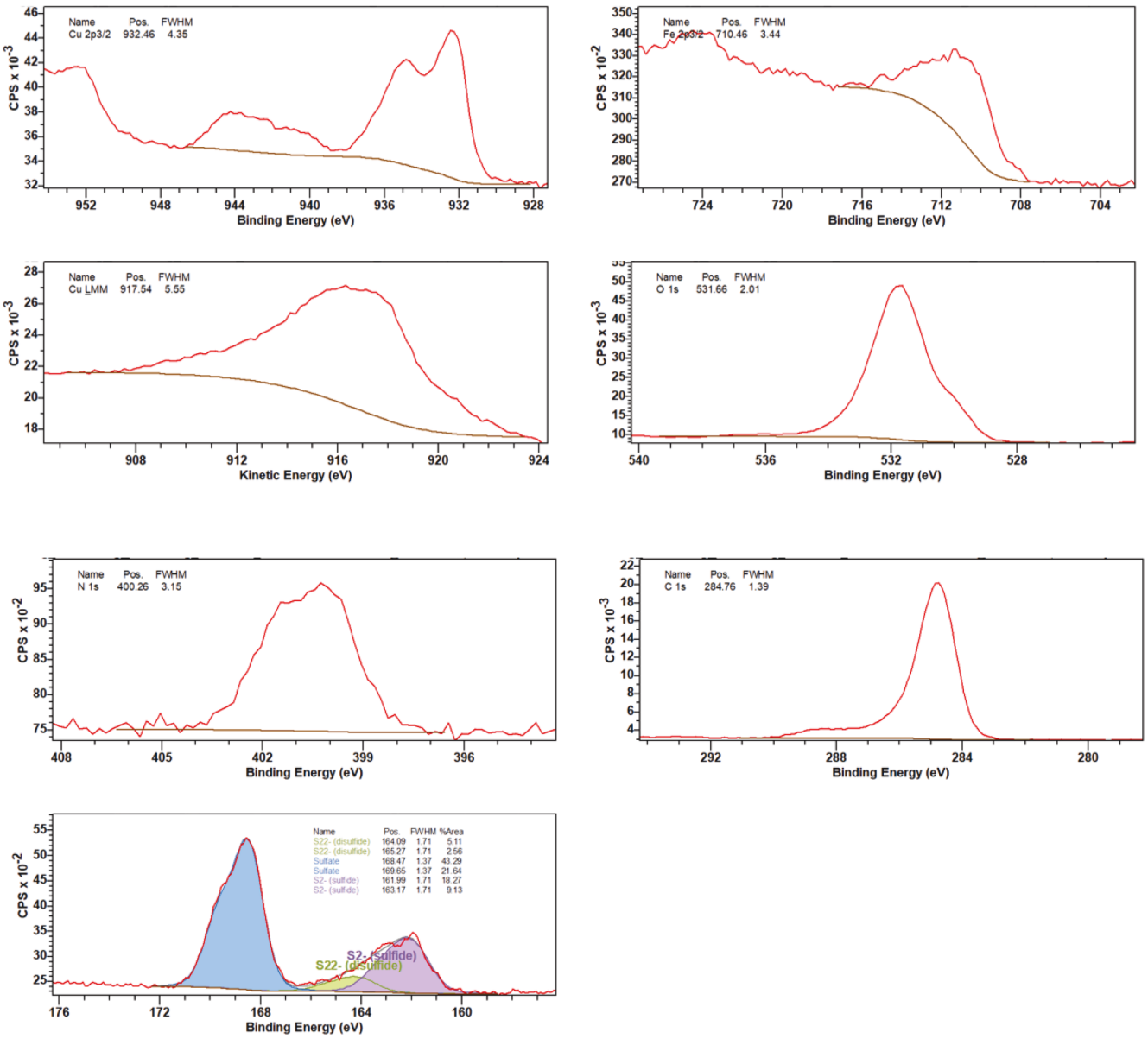

Fig. 4. XPS of Fe_3O_4@$Cu_{2-x}S$ nanoparticles.

Table 1
Optical Properties of the Fe_3O_4@$Cu_{2-x}S$ Film.

Optical property	Value
Solar transmittance	0.18
Solar reflectance (surface with the film)	0.40
Solar absorptance (surface with the film)	0.42
Photopic transmittance	0.33
Photopic reflectance (surface with the film)	0.50
Emissivity (surface with the film)	0.06

provides a summary of the measured photothermal nanofilm's spectral properties that manifest a strong absorption in the NIR and UV regions but fewer effects in the visible region, which is because of the specific response of the synthesized Fe_3O_4@$Cu_{2-x}S$ NPs.

2.3. Numerical model and experimental validation

Solar radiation can be transmitted, reflected, or absorbed in varying amounts, based on the ambient environmental conditions and the window's optical properties. Transmission of solar radiation directly to the indoors of a building can increase cooling loads but reduce space heating needs. Absorption of solar radiation by windows can flow both ways, outward or inward from the panes. The thermodynamic process that occurs on double-pane windows coated with photothermal NPs can include all three types of (thermal) heat transfer: radiative, conductive, and convective. The solar IR absorbed by the photothermal film layer is converted into high-level thermal energy, based on the nanoscale PPE; comparatively, enhanced heat transfer occurs on the film-surface side (i.e., exterior in summer and interior in winter in the reversible window paradigm described in the present research).

When the glazing materials are coated on the surface by plasmonic NPs, the (LSPR-induced) temperature of the PPE may increase significantly on the coated surface, to a fraction of heat flow to the material. This can be defined by the substantial heat transfer minimization occurring between the substrate and NPs that is driven by the quasi-ballistic effect, which results from the situation when the size of the particle is significantly smaller than the phonon mean free path in the substrate material [49]. Inspired by previous research on (LSPR-induced) solar vapor generation [50], a hypothesized interfacial

insulation (R_h) between the glazing and nanoscale coating of plasmonic NPs was incorporated into the traditional heat transfer model (Eq. (1)). In situations involving stable boundaries and the same atmospheric (i.e., ambient temperature) conditions, the (absorbed) solar energy Q_{in} equals the amount of the heat dissipation from the surface of the NP coating and heat transfer through conduction away from the NP-coated surface to the glass, through the interfacial layer. The mathematical expression for Q_{out} is provided below.

$$Q_{out} = h_{con-NP}\left(T_{NP,s} - T_{\infty}\right)A_s + \varepsilon_{NP}\sigma\left({T_{NP,s}}^4 - {T_{\infty}}^4\right)A_s + \left(\frac{1}{R_h}\right)\left(T_{NP,s} - T_{glass,s}\right)A_s \quad (1)$$

where Q_{out} refers to the heat dissipation, including the heat transfer of convection, radiation, and conduction. The temperature of the soda-lime glass surface on the coating side is $T_{glass,s}$ and $T_{NP,s}$ is the coated layer's surface temperature. Thus, ($T_{NP,s}$ - $T_{glass,s}$) is the difference in temperature between the two surfaces (or sides) of the hypothesized interfacial insulation. The ambient air temperature is T_{∞}. The interfacial insulation (R_h) is defined by the attachment of the temperature model of the analytical surface to the surface temperature (i.e., measured) data. The variables $h_{con\text{-}NP}$,ε_{NP} , and σ are the parameters involved in the transfer of heat on the coated surface's photothermal and surrounding elements. Notably, the functioning is different from the traditional model for the macroscopic transfer of heat, where (conductive) heat transfer occurs directly from the (photothermal) coating layer to the glass soda-lime substrate. The existence of interfacial insulation creates barriers to heat flow and then matches with the increased heat dissipation of the coating surface. Also, this interfacial insulation varies with the types, concentration levels, and characteristics of the NPs coated on the surface, which has to be experimentally measured and analytically derived.

Furthermore, to understand the solar heat gain effects formed by the proposed dynamic concept, SHGC has to be computed. In the National Fenestration Rating Council (NFRC) 200 standard for SHGC calculation, SHGC can be determined by the sum of two aspects under standard boundary conditions (i.e., interior ambient temperature of 24 °C, exterior ambient temperature of 32 °C, wind speed of 2.75 m/s, and incident solar irradiance of 783 W/m^2): τ_s solar transmittance and α_s solar absorptance (inward-flowing heat). However, this becomes more complicated when the NIR-absorptive nanofilm is on different surfaces because of its semi-directional photothermal heating feature. In other words, the SHGC calculation completed using standardized boundary conditions may not be accurate for the present research. Therefore, we adopted another set of equations for the SHGC calculation, as follows:

$$Q_{solar\ gains} = \mathrm{h}_i A_s\left(T_{in,s} - T_i\right) + \varepsilon_i\sigma A_s\left({T_{in,s}}^4 - {T_i}^4\right) \quad (2)$$

$$SHGC = \left(Q_{solar\ gains} - Q_{U-factor}\right)/\int A_s G_{\lambda} \quad (3)$$

where $Q_{solargains}$ is the sum of the inward-flowing heat flux (both convection and radiation) obtained by the given solar irradiation and indoor temperature condition T_i, and $T_{in,s}$ is the window's inner surface temperature, which will be calculated from Eq. (1). The overall inward-flowing heat flux is not only the result of solar radiation but also the air temperature difference between indoors and outdoors. To calculate the pure solar heat gain, the amount of heat flux by the temperature differences needs to be subtracted. As shown in Eq. (3), $Q_{U-factor}$ is the U-factor-driven heat flux resulting from the temperature difference between the indoor and outdoor air, and $\int A_s G_{\lambda}$ is used to calculate the overall solar irradiance incident on the window.

To validate the numerical equations above, the same boundary conditions (i.e., ambient air temperature of 298 K and relative humidity of 30%) and material properties measured in the above experiments (i.e., solar absorptance: ~0.22, thermal conductivity of the glass: 0.8 W/(m·K), and dimensions of the Fe_3O_4@$Cu_{2-x}S$ NP-coated glass: 0.0254 * 0.0254 m^2) were used in the analytical model. The experiment setup and workflow can be found in Fig. 5. The power density on the samples from the solar simulator was 0.1 W/cm^2. For the heating curves, the temperatures of the samples were recorded every minute for the first 10 min. Then the light source was turned off. Different concentrations of NPs were used to develop samples with different visible and solar transmittances. An IR camera (FLIR E6) was used to record the temperature of the samples. To minimize light reflection, a black sheet was placed under the sample. An optical power meter (Coherent Inc.) was used to calibrate the power density of the solar simulator. There were two main steps: cooling and heating.

3. Results and discussion

This section describes the results of the above numerical model validation and the whole building energy performance of the reversible photothermal windows by incorporating the validated model.

3.1. Interfacial insulation and model validation

The hypothesized interfacial insulation value R_h (0.117 m^{2}K/W) was determined by fitting the analytically calculated surface temperature to the measured temperature data at the steady-state status and 0.1 W/cm^2 solar irradiance. Subsequently, this parameter was incorporated into the analytical model with different solar absorptance levels, which yielded a series of time-dependent temperature increase data. The comparison was made between the calculated and measured temperature increase data under different solar absorptance levels (see Fig. 6), which showed that the proposed analytical model was in good agreement (~0.07 mean relative error and 0.99 R-squared) with the photothermal experimental data.

3.2. Thermal and optical properties of reversible Double-Pane photothermal windows

First, the measured spectral data for the plasmonic nanofilm (Fe_3O_4@$Cu_{2-x}S$ NPs) were applied to a double-pane window (4 mm clear glass panes with 12 mm air gap) to calculate the resulting optical properties via LBNL WINDOW software. The LBNL WINDOW software implements the ISO 15099 window calculation standard [51] and is also certified by the NFRC [52], which can accurately (1–2% errors) compute the transmittance and reflectance as a function of the wavelength of multiple-layer glazing structures as long as each layer's optical data are measured and imported [53]. Fig. 7 presents the spectral absorptance and transmittance of two different nanofilm placements: internal and external surfaces targeted for summer and winter, respectively. The features of the spectral absorptance for the two placements were similar, especially for the NIR portion, while the absorptance was relatively higher when the film was placed inside. This can be explained by the reflective feature of the nanofilm, which becomes effective when it is directly exposed to the exterior. Also, there was little or no change in the visible transmittance of the reversible photothermal windows, regardless of whether the nanofilm was coated on the external or internal surfaces.

Regarding the thermal properties, LBNL WINDOW could also be used to calculate the center-of-glass U-factor of the designed glazing models, following the National Fenestration Rating Council (NFRC) and ISO 15099 standards. The environmental condition settings for the U-factor calculations for these standards include an interior ambient temperature of 21 °C, exterior ambient temperature of −18 °C, and wind speed of 5.5 m/s. In the reversible design, although the materials and structures are the same for the two nanofilm placements, the surface heat transfer (by both radiation and convection) with the ambient conditions are still different, leading to differences in the resultant U-factor. In particular, since the nanofilm has a low emissivity feature (~0.06), its surface heat transfer (both radiative and convective) was determined to be relatively

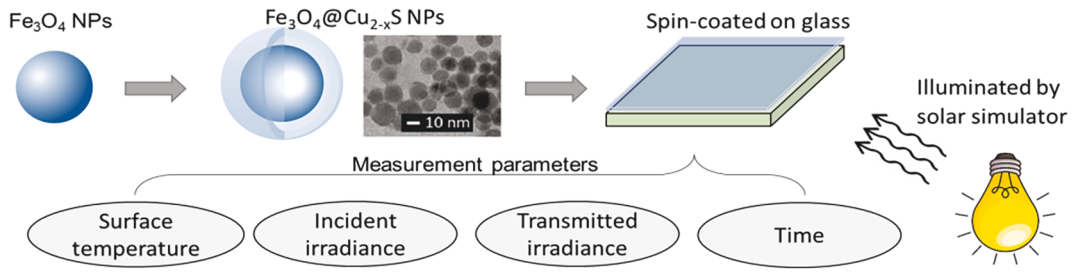

Fig. 5. Experiments for validation.

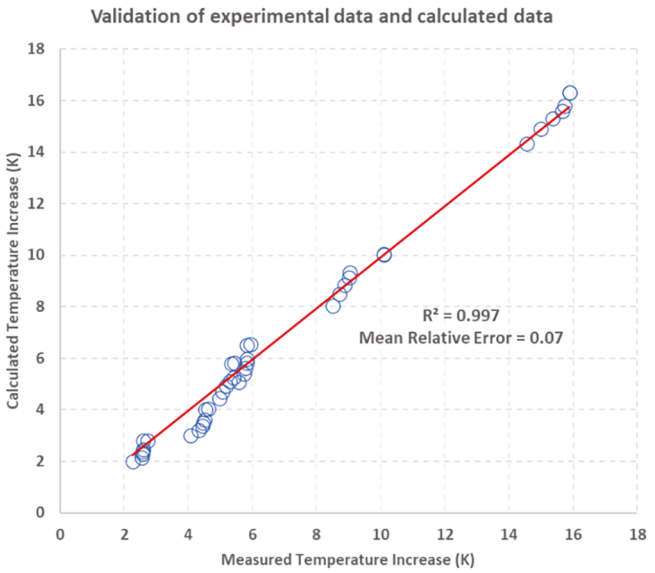

Fig. 6. Analytical model validation using experimental data.

lower when the nanofilm was coated on the internal rather than the external surface. Accordingly, the center-of-glass U-factor of the internal nanofilm placement (for winter) calculated and reported by the program was lower than for the external nanofilm placement (for summer). The major thermal and optical properties of the two nanofilm placements are provided in Table 2.

3.3. Seasonal characteristics of solar heat gain coefficient

The analytical model validated in Section 2 was used to conduct a numerical analysis of the SHGC value variations for the reversible photothermal window during different seasons. Solar irradiance values ranged from 100 W/m^2 to 1,000 W/m^2, with a 50 W/m^2 interval. Outdoor temperatures ranged from 258 K to 313 K, with a 3-degree interval. The indoor air conditions were maintained at 297 K. As such, 399 boundary combinations were formed and used to calculate two situations: internal and external placement of the nanofilm on double-pane windows.

Two major features can be seen in Fig. 8 above. First, the SHGC values in the two situations generally had different bands. The values ranged from 0.20 to 0.23 when the nanofilm was coated on the window's outer surface, and from 0.48 to 0.60 when the nanofilm was placed on the inner surface. Such variations by nanofilm placement are quite aligned with the initial concept design for the reversible window: higher SHGC in winter and lower SHGC in summer. Little or no difference in the visible transmittance and visual quality was found between the seasons. To explain the underlying mechanism causing such variations, both the photothermal effects and LSPR-driven semi-directional heat transport needed to be taken into account. The absorbed solar IR on the nanofilm was converted into thermal energy and then dissipated to the ambient environment. The existence of the air gap played an important role in strengthening the directional heat flow. In summer, more heat flux was released to the outdoors and prevented from entering the interior via the air gap insulation. More heat was contained by the air gap insulation and then flowed inward. The presence of the interfacial insulation resulting from the nanoscale PPE further enhanced the heat

Table 2
Major Thermal and Optical Characteristics of the Reversible Photothermal Nanofilms.

Window property	Internal placement	External placement
U-factor	1.89	2.69
Visible transmittance VT, 380–780 nm	0.32	0.32
Solar transmittance τ_s, 300–2,500 nm	0.15	0.15
Solar absorptance, 300–2,500 nm	0.73	0.45
NIR transmittance, 780–2,500 nm	0.10	0.08
NIR absorptance, 780–2,500 nm	**0.80**	**0.63**
Front emissivity (outward)	0.84	0.06
Back emissivity (inward)	0.06	0.84

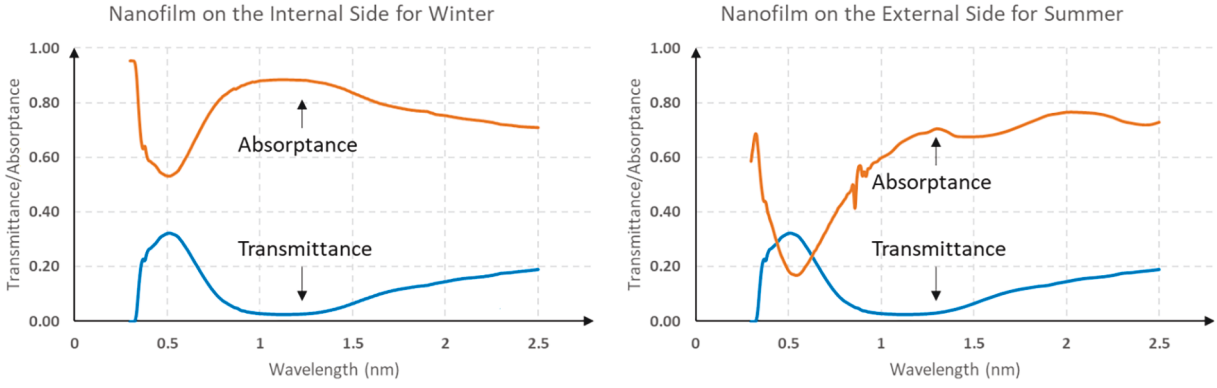

Fig. 7. Optical characteristics of double-pane windows coated with nanofilms on the internal (left) and external layers (right).

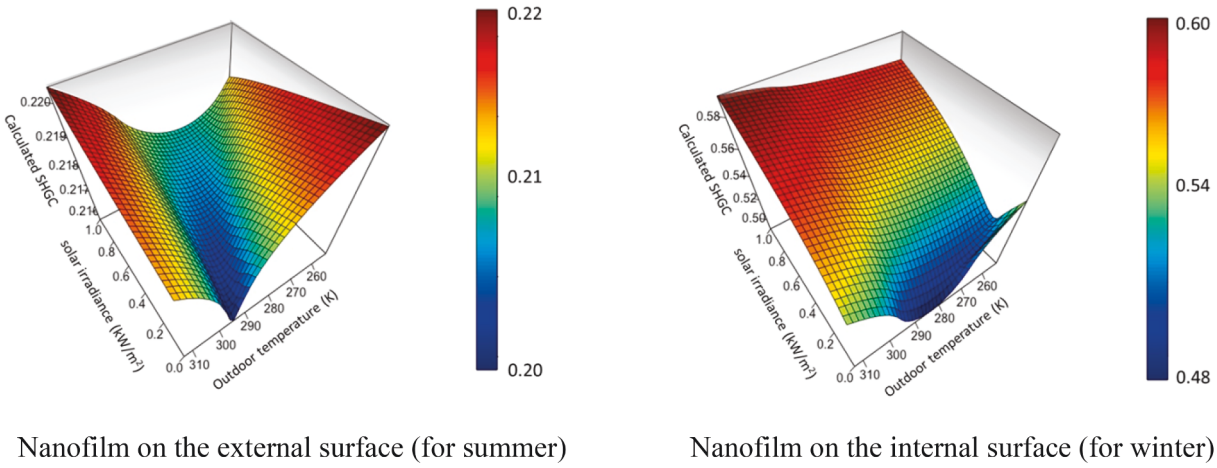

Fig. 8. SHGC data distribution for the photothermal window in summer (left) and winter (right).

flow modulation, making even more heat dissipate outward in summer and flow inward in winter. Second, the SHGC values depended on the external boundary conditions and showed complicated variations, roughly along a parabolic surface. When the temperature difference between the inner window surface and interior was comparatively small, a lower heat flux flowed inward, and then lower SHGC values were obtained. This variation trend is similar to what was seen for the two nanofilm placements and more obvious for the internal placement. This again verifies the assumption that a single SHGC value calculated within standardized condition boundaries could not represent the actual solar heat gain variations of the photothermal window, due to its strong solar absorption and the presence of interfacial insulation resulting from the nanoscale PPE.

Based on 798 data points obtained from the above numerical analyses, two regression statistical models for summer and winter SHGC (denoted as $SHGC_{PPE}$, indicating the nanoscale PPE feature) were developed and are expressed below.

$$SHGC_{PPE} = 1 - \frac{1}{1 + e^{a*T_o + b*G_0}} \tag{4}$$

where G_0 is the total incident solar irradiance and T_o is the outdoor temperature. For the summer SHGC model, $a = -4.414 \times 10^{-3}$ and $b = -3.724 \times 10^{-2}$. For the winter SHGC model, $a = 3.235 \times 10^{-4}$ and $b = 2.603 \times 10^{-1}$. The adjusted R-squared values for the summer and winter SHGC models were 0.99 and 0.97, respectively. The agreement plots for the model testing are shown in Fig. 9, which also verifies the high accuracy of the two regression models obtained.

3.4. Comparison with representative dynamic glazing systems

The SHGC and visible transmittance values of this design are plotted in Fig. 10, in which some representative chromic-based glazing properties in Section 1 are also added for the comparative purpose. The lines represent the glazing property change (SHGC and visible transmittance) in two statuses (e.g., clear and tinted), and it shows the positive and linear correlations between the values of SHGC and visible transmittance in most dynamic glazing systems. In particular, achieving the low SHGC in summer seasons in these existing dynamic technologies has to be coupled with low visible transmittance and visual appearance (e.g., color, clarity), which may further negatively affect indoor electrical lighting energy use and daylighting and window view benefits to indoor occupants. Comparatively, the proposed reversible photothermal windows may realize the SHGC control (0.2–0.6) in different seasons without affecting the visible transmittance (0.32) and visual appearance. As discussed in Section 1, decoupling the SHGC and visible light control would enable independent solar heat gain modulation in different seasons and allow daylighting benefits throughout the year, which is particularly important for commercial buildings that are occupied during daylight hours. When the glazing system is physically reversed, both solar and visible transmittance values are kept the same but the inward thermal flow is significantly altered due to the change of

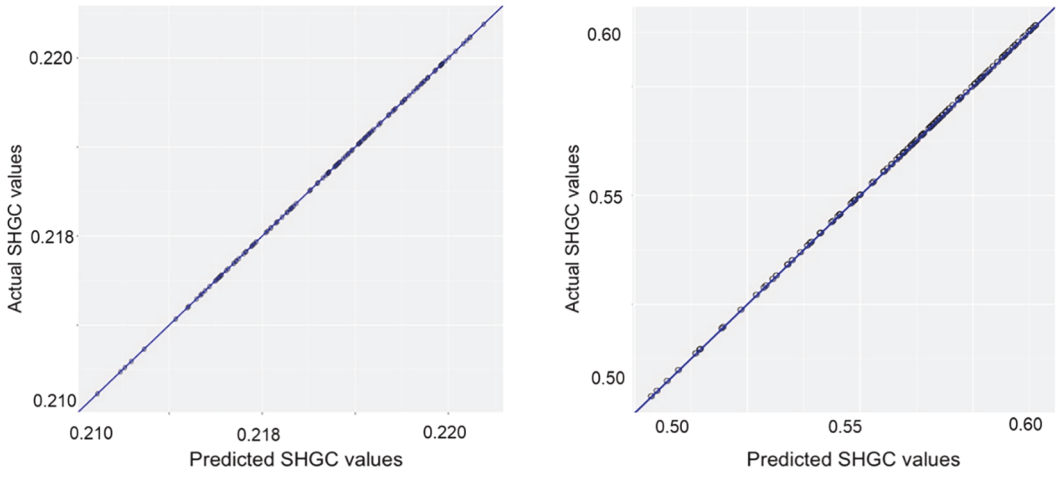

Fig. 9. Agreement plots of model testing.

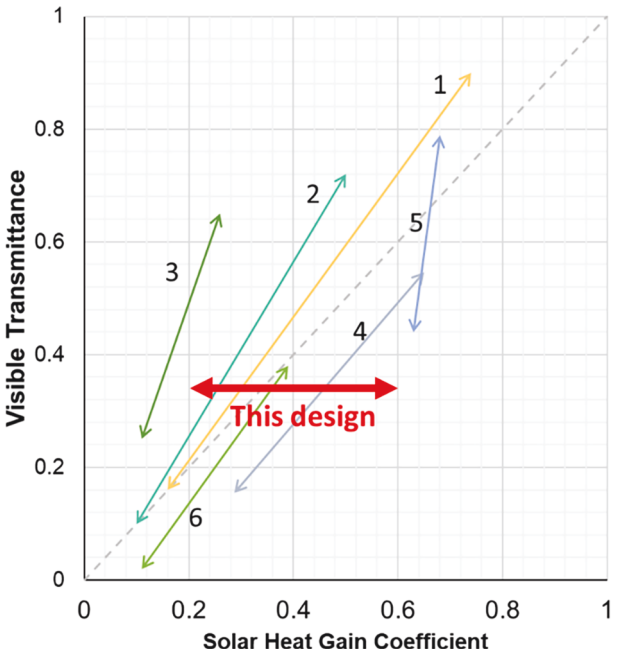

Fig. 10. SHGC vs. Visible Transmittance (1-[27], 2-[28], 3-[29], 4-[30], 5-[31], 6-[32]).

the nanofilm placement, which forms the large difference in SHGC.

3.5. Effects on building heating, cooling, and lighting energy use

In this section, the previous method of parametric energy simulation was followed to incorporate the dynamic SHGC features of the reversible photothermal window into the whole-building energy simulation [54]. This parametric energy simulation method was based on the Energy Management System (EMS) module in Energy Plus [55], in which the SHGC value of the building window could be changed, by following Eq. (4), in response to external conditions of outdoor air temperature and incident solar irradiance. The regression models established above were embedded into the EMS module and used to determine the SHGC values.

The prototype models (small 1-story office with ~ 510 m^2 floor area) were developed by the Department of Energy for use by researchers in comparing design alternatives, assessing new technologies, optimizing system controls, and developing energy codes and standards. To understand the potential for energy savings offered by the proposed reversible photothermal windows, the prototype models that follow the ASHRAE 90.1–2019 building energy efficiency standard as a baseline were used. In these models, all window thermal and optical properties were defined and had different levels that depended on climatic conditions. Although it was expected that the proposed reversible photothermal windows would not be beneficial in all climatic conditions, the comparisons across eight US climate zones provided a more comprehensive understanding of the potential energy savings. The window properties used in this analysis are shown in Table 3.

Furthermore, the preliminary analyses were conducted on the selection of "switching" months for each climate, based on the simulation data. As shown in the following diagram (Fig. 11), the procedure was first to simulate the monthly heating and cooling energy use for each window mode (summer and winter) and then compare the monthly energy use between the two. Finally, the optimal seasonal operation modes for the reversible photothermal window could be determined. In this seasonal operation, one manually flips the window system only twice a year. Adopting the seasonal control described in this work avoids complications related to an optimization analysis and simply reveals the major trends and potential for using reversible photothermal windows. Further discussion regarding optimization can be found in the conclusion.

Table 3
Window Properties Used in the Whole Building Energy Analysis.

Climate Zone	U-factor (W/m^2K)	Solar Heat Gain Coefficient	Visible Transmittance
1A-Honolulu, HI	2.84	0.23	0.25
2B-Tucson, AZ	2.62	0.25	0.28
3B-El Paso, TX	2.39	0.25	0.28
4B-Alburquerque, NM	2.05	0.36	0.39
5B-Denver, CO	2.05	0.37	0.42
6B-Great Falls, MT	1.93	0.37	0.42
7-International Falls, MN	1.65	0.39	0.44
8-Fairbanks, AK	1.48	0.40	0.44
Reversible Photothermal Window			
Summer	2.69	0.20–0.23	0.32
Winter	1.89	0.48–0.60	0.32

Using the procedure outlined above, we identified the optimal operation modes for the reversible photothermal windows for each climatic zone. Fig. 12 clearly shows how the reversible photothermal window concept can be effective and applicable in different climates. In hot climates such as Zones 1 and 2, there was no need to dynamically operate the window SHGC, since the low SHGC window performed better all year along. In all other climates, switching to the high SHGC in certain months was found to be desirable. In cold climates (i.e., Zones 7 and 8), setting the reversible photothermal windows at a high SHGC mode was the major operation.

More detailed energy use analyses were conducted based on the simulation results in terms of heating, cooling, and lighting energy use. Fig. 13 depicts comparisons of the baseline model and model with reversible photothermal windows for each climatic zone. In general, the reversible photothermal windows consistently saved annual energy use (heating, cooling, and lighting), with 1.2% to 18.2% savings relative to the baseline models. However, combined with the seasonal operation modes discussed above, it can be seen that the energy savings in Zones 1 and 2 were not due to the dynamic SHGC feature, but rather its lower U-factor and higher visible transmittance. More pronounced energy savings provided by the dynamic SHGC in different seasons could be observed in mixed climates (i.e., Zones 5 and 6), approximately 18%. If only heating and cooling energy use were considered, the energy savings provided by the dynamic SHGC reached approximately 25%.

4. Conclusion

In the present research, a new type of dynamic window was designed and demonstrated to incorporate plasmonic photothermal effects and control solar heat gain in response to different seasons while maintaining stable and sufficient visible transmittance for potential daylighting benefits and lighting energy savings. This dynamic SHGC control fashion in the building window area has not been achieved yet in previous works. The proposed system can achieve the SHGC variation of 0.2–0.6 with a stable visible transmittance of 0.32. To understand its underlying mechanism of dynamic solar heat gain control, an analytical model was built, experimentally validated, and used in a series of numerical analyses. Because of the semi-directional heat transport feature formed by the plasmonic film under solar radiation, combined with the insulating function of the air gap of double-pane windows, the inward-flowing heat converted from the absorbed solar NIR energy (60 ~ 80% absorption) was able to be modulated in different climates by switching the film's placement (i.e., external or internal surface of the window). The level of visible transmittance was maintained in each placement. In other words, the principal mechanism of the dynamic SHGC for this type of window relies on the solar NIR portion's absorption and thermal transport modulation, independent of the visible light portion. The

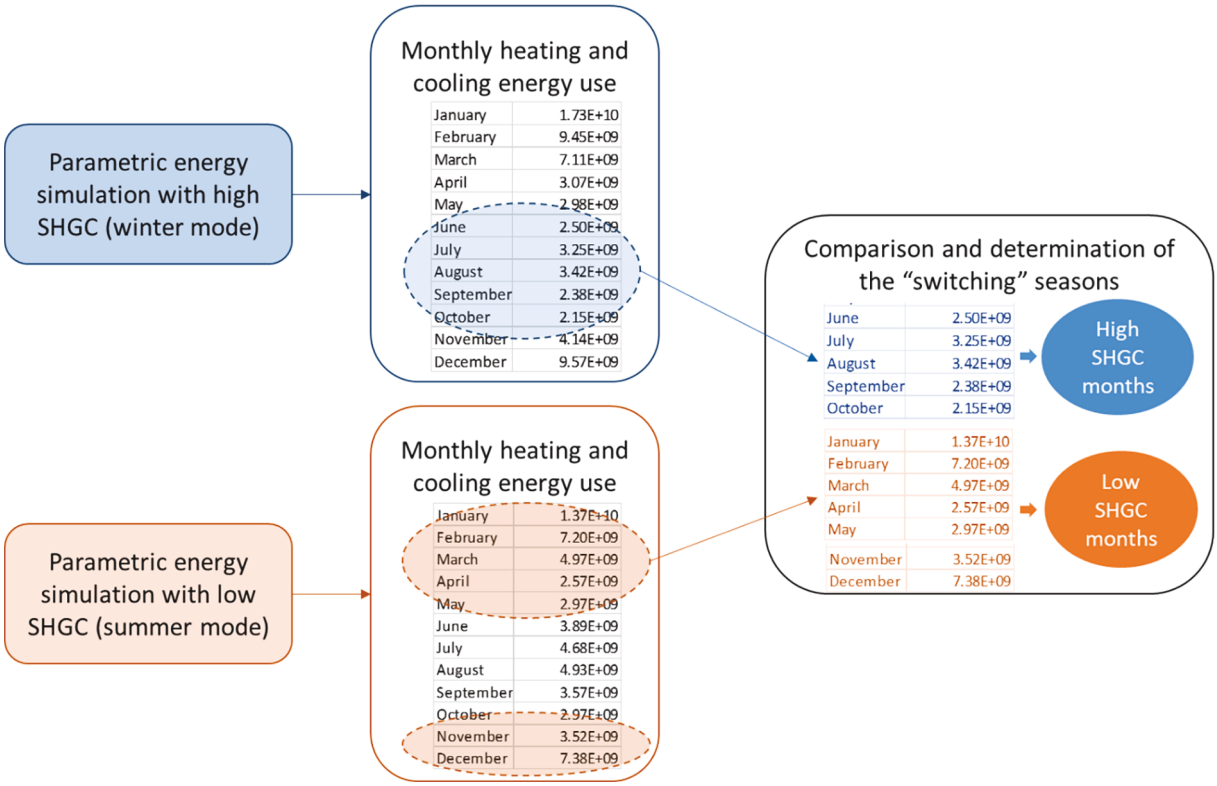

Fig. 11. Procedure for determining the optimal seasonal operation for reversible photothermal windows.

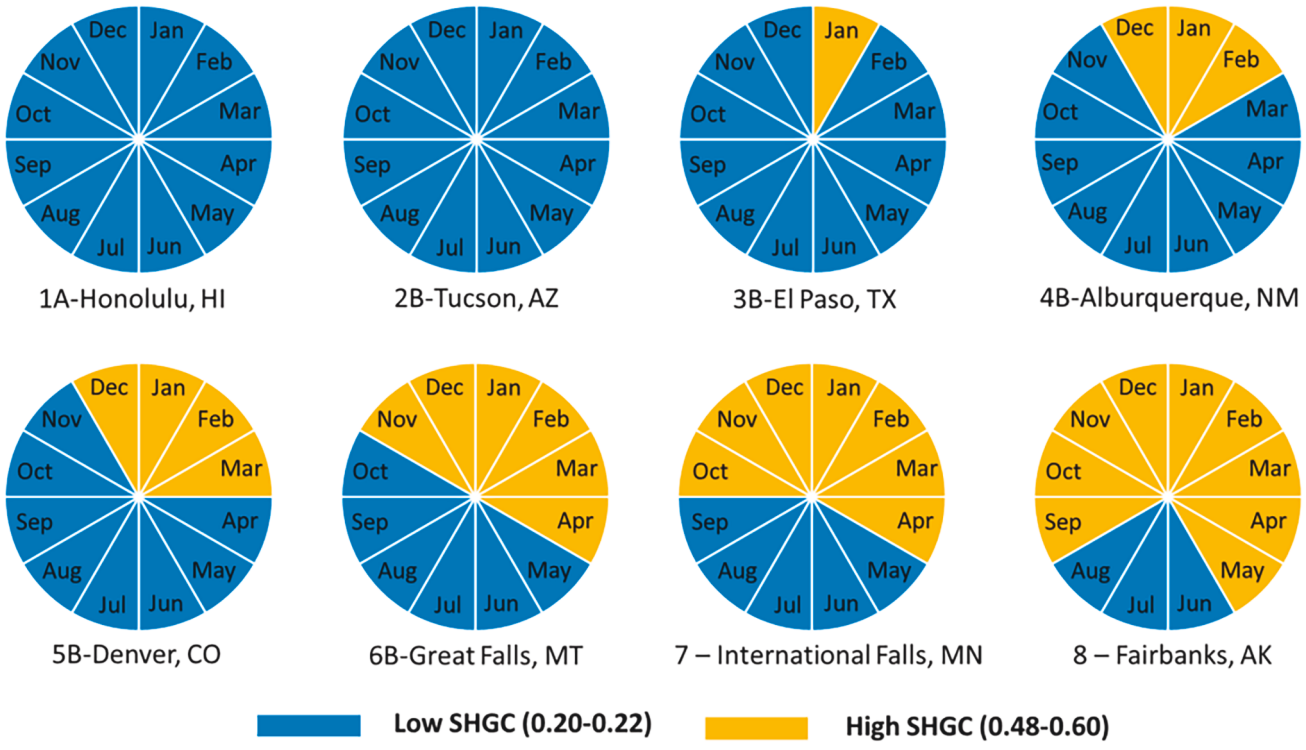

Fig. 12. Optimal seasonal operation (in months) for the reversible photothermal windows.

parametric energy simulation method was employed in *EnergyPlus* to take dynamic SHGC models into account and demonstrated that above **18%** energy savings can be obtained in mixed climates by using reversible photothermal windows (as compared to DOE prototype models). In hot and cold climates, the energy savings were minor, ranging from **1.2% to 7%.**

It is important to mention that there are a few optimization-related issues for this technology that were not considered to be within the

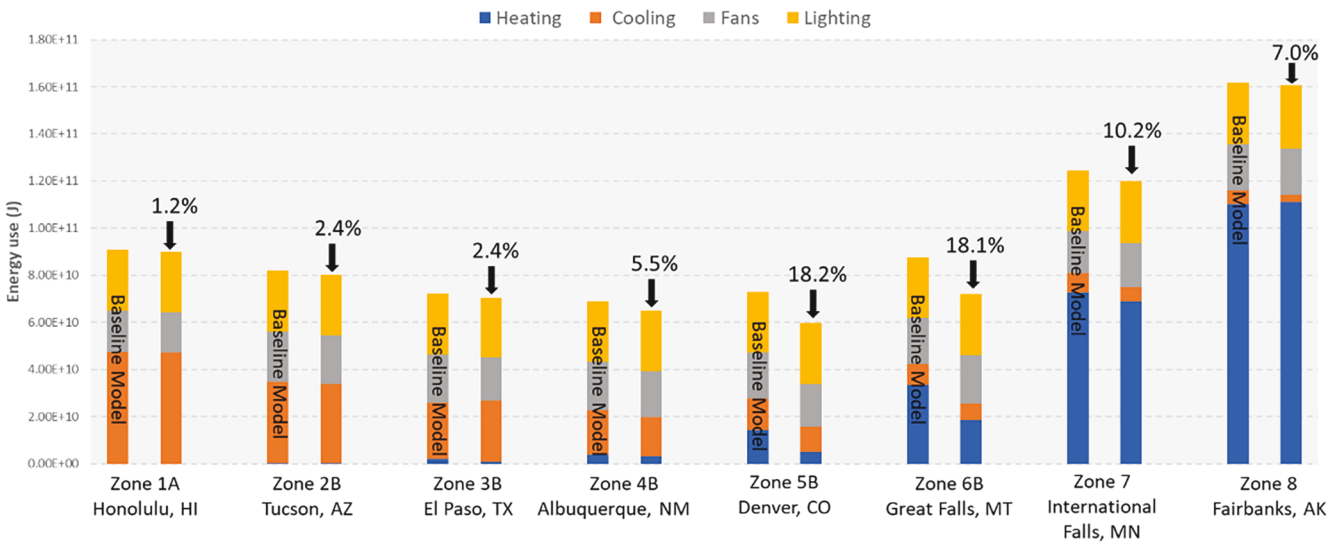

Fig. 13. Percentages of energy savings for reversible photothermal windows across different climates.

scope of this research but can be conducted in the future. First, the spectral selectivity of the system can be determined by synthesizing different sizes and shapes of plasmonic NPs, a topic that has been discussed extensively in prior studies about nanomaterial science and engineering but not included in this work. By fine-tuning the spectral region and peak, the uncoupled mode of solar NIR absorption and visible transmittance can be further enhanced, and more energy savings possibly achieved. Second, the heating-dominated and cooling-dominated climates have a relatively lower potential for energy savings, which may be due to the dynamic SHGC range (i.e., 0.2 to 0.6) used in this work. By adjusting the concentration levels of the plasmonic NPs, the SHGC range can be conveniently controlled, and certain ranges of dynamic SHGC may achieve higher energy savings in these climates. Third, to simplify the demonstration of the technology, a monthly energy use comparison between the high and low SHGC values was adopted, meaning that maybe some important within-month temperature variations were missed. Ideally, if the overall reversible window system can be motorized and actuated by the indoor heating/cooling demands and outdoor conditions, more substantial energy savings can be expected. The optimal configurations and controls can be determined by coupling the two developed $SHGC_{PPE}$ models (i.e., high and low SHGC models in Eq. (4)) and incorporating them into the parametric energy simulation procedure. These optimization-related questions above will be explored in future work. Finally, to demonstrate the implementability of the reversible photothermal window, physical prototypes with all necessary window assemblies (for reversible operation) need to be fabricated and examined in terms of its potential infiltration effects, optimal operation mode, and solar angle dependence of light-to-heat conversion, etc.

CRediT authorship contribution statement

Md Anwar Jahid: Material characterization, Investigation. **Julian Wang:** Conceptualization, Methodology, Project administration, Mathematical models. **Enhe Zhang:** Experiments, Numerical simulation, Validation. **Qiuhua Duan:** Energy simulation. **Yanxiao Feng:** Visualization.

Declaration of Competing Interest

The authors declare that they have no known competing financial interests or personal relationships that could have appeared to influence the work reported in this paper.

Acknowledgements

We acknowledge the financial support provided by the National Science Foundation CMMI-2001207 and National Science Foundation CMMI-1953004. We thank Dr. Donglu Shi's research group at the University of Cincinnati for providing the material samples. We also need to acknowledge the support of the Material Characterization Laboratory of Penn State Materials Research Institute.

References

[1] Hepbasli A. Low exergy (LowEx) heating and cooling systems for sustainable buildings and societies. Renew Sustain Energy Rev 2012;16(1):73–104.
[2] Carmody J, Haglund K, Guideline M. Energy-Efficient Window Performance and Selection. NorthernSTAR, University of Minnesota, Building Technologies program 2012, U.S. Department of Energy.
[3] Brzezicki M. A systematic review of the most recent concepts in smart windows technologies with a focus on electrochromics. Sustainability 2021;13:9604.
[4] Andow BC, Krietemeyer B, Stark PRH, Dyson AH. Performance criteria for dynamic window systems using nanostructured behaviors for energy harvesting and environmental comfort. In Proceedings of the SPIE 8692, Sensors and Smart Structures Technologies for Civil, Mechanical, and Aerospace Systems, San Diego, CA, USA, 10–14 March 2013.
[5] Harris C, LaFrance M, Sawyer K. Emerging Technologies Research and Development, DRAFT Research and Development Opportunities Report for Windows, US department of energy, May 2020.
[6] Hammarberg E, Roos A. Antireflection treatment of low-emitting glazings for energy efficient windows with high visible transmittance. Thin Solid Films 2003;442(1–2):222–6.
[7] Rosencrantz T, Bülow-Hübe H, Karlsson B, Roos A. Increased solar energy and daylight utilisation using anti-reflective coatings in energy-efficient windows. Sol Energy Mater Sol Cells 2005;89(2–3):249–60.
[8] Durrani SMA, Khawaja EE, Al-Shukri AM, Al-Kuhaili MF. Dielectric/Ag/dielectric coated energy-efficient glass windows for warm climates. Energy Build 2004;36(9):891–8.
[9] Cheng CH, Ting JM. Transparent conducting GZO, Pt/GZO, and GZO/Pt/GZO thin films. Thin Solid Films 2007;516(2–4):203–7.
[10] Zinzi M. Office worker preferences of electrochromic windows: a pilot study. Build Environ 2006;41(9):1262–73.
[11] Granqvist CG. Handbook of inorganic electrochromic materials. Elsevier Science Ltd 1995.
[12] Lee ES, DiBartolomeo D. Application issues for large-area electrochromic windows in commercial buildings. Sol Energy Mater Sol Cells 2002;71(4):465–91.
[13] Wittwer V, Datz M, Ell J, Georg A, Graf W, Walze G. Gasochromic windows. Sol Energy Mater Sol Cells 2004;84(1-4):305–14.
[14] Baetens R, Jelle BP, Gustavsen A. Properties, requirements and possibilities of smart windows for dynamic daylight and solar energy control in buildings: a state-of-the-art review. Sol Energy Mater Sol Cells 2010;94(2):87–105.
[15] Tao Y, Fang X, Zhang H, Zhang G, Tu J, Shi L. Impacts of thermo-optical properties on the seasonal operation of thermochromic smart window. Energy Convers Manage 2022;252:115058.
[16] Li ZX, Abdullah AAA, Al-Rashed RM, Kalbasi R, Shahsavar A, Afrand M. Heat transfer reduction in buildings by embedding phase change material in multi-layer

walls: effects of repositioning, thermophysical properties and thickness of PCM. Energy Convers Manage 2019;195:43–56.
[17] Sadineni SB, Madala S, Boehm RF. Passive building energy savings: a review of building envelope components. Renew Sustain Energy Rev 2011;15(8):3617–31.
[18] Solovyev AA, Rabotkin SV, Kovsharov NF. Polymer films with multilayer low-E coatings. Mater Sci Semicond Process 2015;38:373–80.
[19] Huang S, Wang Z, Xu J, Lu D, Yuan T. Determination of optical constants of functional layer of online Low-E glass based on the Drude theory. Thin Solid Films 2008;516(10):3179–83.
[20] Schaefer C, Bräuer G, Szczyrbowski J. Low emissivity coatings on architectural glass. Surf Coat Technol 1997;93(1):37–45.
[21] Aburas M, Soebarto V, Williamson T, Liang R, Ebendorff-Heidepriem H, Wu Y. Thermochromic smart window technologies for building application: a review. Appl Energy 2019;255:113522.
[22] Ji J, Zhou S, Wang W, Ling F, Yao J. Active control of terahertz plasmon-induced transparency in the hybrid metamaterial/monolayer MoS2/Si structure. Nanoscale 2019;11(19):9429–35.
[23] Zaki OM, Mohammed RH, Abdelaziz O. Separate sensible and latent cooling technologies: A comprehensive review. Energy Convers Manage 2022;256:115380.
[24] Chow TT, Li C, Lin Z. Innovative solar windows for cooling-demand climate. Sol Energy Mater Sol Cells 2010;94(2):212–20.
[25] Li C, Tan J, Chow TT, Qiu Z. Experimental and theoretical study on the effect of window films on building energy consumption. Energy Build 2015;102:129–38.
[26] Qahtan AM. Thermal performance of a double-skin façade exposed to direct solar radiation in the tropical climate of Malaysia: A case study. Case Stud Thermal Eng 2019;14:100419.
[27] Allen K, Connelly K, Rutherford P, Wu Y. Smart windows—dynamic control of building energy performance. Energy Build 2017;15(139):535–46.
[28] Hoon Lee J, Jeong J, Tae Chae Y. Optimal control parameter for electrochromic glazing operation in commercial buildings under different climatic conditions. Appl Energy 2020;260:114338.
[29] Wu YL, Zhao Q, Huang H, Jeremy R, Lim W. Sol-gel based photochromic coating for solar responsive smart window. Surf Coat Technol 2017;320:601–7.
[30] Feng W, Zou L, Gao G, Wu G, Shen J, Li W. Gasochromic smart window: optical and thermal properties, energy simulation and feasibility analysis. Sol Energy Mater Sol Cells 2016 Jan;1(144):316–23.
[31] Hemaida A, Ghosh A, Sundaram S, Mallick TK. Evaluation of thermal performance for a smart switchable adaptive polymer dispersed liquid crystal (PDLC) glazing. Sol Energy 2022;195:185–93.
[32] Nundy S, Ghosh A. Thermal and visual comfort analysis of adaptive vacuum integrated switchable suspended particle device window for temperate climate. Renew Energy 2020;1(156):1361–72.
[33] Duan Q, Feng Y, Wang J. Clustering of visible and infrared solar irradiance for solar architecture design and analysis. Renew Energy 2021;165:668–77.
[34] Lin KT, Lin H, Jia B. Plasmonic nanostructures in photodetection, energy conversion and beyond. Nanophotonics 2020;9(10):3135–63.
[35] Berweger S, Atkin JM, Olmon RL, Raschke MB. Light on the tip of a needle: plasmonic nanofocusing for spectroscopy on the nanoscale. J Phys Chem Lett 2012; 2012(3):945–52.
[36] Kelly KL, Coronado E, Zhao LL, Schatz GC. The optical properties of metal nanoparticles: the influence of size, shape, and dielectric environment. J Phys Chem B 2003;107:668–77.
[37] Brongersma ML, Halas NJ, Nordlander P. Plasmoninduced hot carrier science and technology. Nat Nanotechnol 2015;10(1):25–34.
[38] Mubeen S, Lee J, Singh N, Krämer S, Stucky GD, Moskovits M. An autonomous photosynthetic device in which all charge carriers derive from surface plasmons. Nat Nanotechnol 2013;8(4):247–51.
[39] Park J-E, Kim M, Hwang J-H, Nam J-M. Golden opportunities: plasmonic gold nanostructures for biomedical applications based on the second near-infrared window. Small Methods 2017;1(3):1600032.
[40] Virk M, Xiong K, Svedendahl M, Käll M, Dahlin AB. A thermal plasmonic sensor platform: resistive heating of nanohole arrays. Nano Lett 2014;14(6):3544–9.
[41] Kim M, Lee JH, Nam JM. Plasmonic photothermal nanoparticles for biomedical applications. Adv Sci 2019;6(17):1900471.
[42] Li S. VO2-based thermochromic and nanothermochromic materials for energy-efficient windows: computational and experimental studies. Acta Universitatis Upsaliensis 2013.
[43] Garcia G, Buonsanti R, Llordes A, Runnerstrom EL, Bergerud A, Milliron DJ. Near-infrared spectrally selective plasmonic electrochromic thin films. Adv Optical Mater 2013;1(3):215–20.
[44] Williams TE, Chang CM, Rosen EL, Garcia G, Runnerstrom EL, Williams BL, et al. NIR-Selective electrochromic heteromaterial frameworks: a platform to understand mesoscale transport phenomena in solid-state electrochemical devices. J Mater Chem C 2014;17:3328–35.
[45] Kim J, Ong GK, Wang Y, LeBlanc G, Williams TE, Mattox TM, et al. Nanocomposite architecture for rapid, spectrally-selective electrochromic modulation of solar transmittance. Nano Lett 2015;15(8):5574–9.
[46] DeForest N, Shehabi A, Selkowitz S, Milliron DJ. A comparative energy analysis of three electrochromic glazing technologies in commercial and residential buildings. Appl Energy 2017;192:95–109.
[47] Zhang E, Duan Q, Wang J, Zhao Y, Feng Y. Experimental and numerical analysis of the energy performance of building windows with solar NIR-driven plasmonic photothermal effects. Energy Convers Manage 2021;245:114594.
[48] Lin J, Zhao Y, Shi D. Optical thermal insulation via the photothermal effects of Fe3O4 and Fe3O4@Cu2−xS thin films for energy-efficient single-pane windows. MRS Commun 2020;10(1):155–63.
[49] Chen G. Nonlocal and nonequilibrium heat conduction in the vicinity of nanoparticles. J Heat Transfer 1996;118(3):539–45.
[50] Neumann O, Urban AS, Day J, Lal S, Nordlander P, Halas NJ. Solar vapor generation enabled by nanoparticles. ACS Nano 2013;7(1):42–9.
[51] ISO15099. ISO15099:2003, Thermal performance of windows, doors and shading devices - detailed calculations. Indian Ceram 2003, ICS:91.060.50 doors and windows.
[52] Curcija DC, Zhu L, Czarnecki S, Mitchell RD, Kohler C, Simon V, Huizenga C. BERKELEY LAB WINDOW. 2015, code ID-54873, USA.
[53] Rubin M, Powles R. Optical properties of glazing materials at normal incidence (No. LBNL-48322; OM-434). Lawrence Berkeley National Lab.(LBNL), Berkeley, CA (United States) 2001.
[54] Duan Q, Zhang E, Hinkle L, Wang J. Parametric energy simulation methods for solar-NIR selective glazing systems. J Phys Conf Ser 2021;2069(1):012129.
[55] Wang JJ, Beltran L. A method of energy simulation for dynamic building envelopes. Conf Proc Ashrae 2016;6:1–6.